JACS
JOURNAL OF THE AMERICAN CHEMICAL SOCIETY

Communication

pubs.acs.org/JACS

Structural Correlations in Heterogeneous Electron Transfer at Monolayer and Multilayer Graphene Electrodes

Aleix G. Güell, Neil Ebejer, Michael E. Snowden, Julie V. Macpherson, and Patrick R. Unwin*

Department of Chemistry, University of Warwick, Coventry, CV4 7AL, United Kingdom

Supporting Information

ABSTRACT: As a new form of carbon, graphene is attracting intense interest as an electrode material with widespread applications. In the present study, the heterogeneous electron transfer (ET) activity of graphene is investigated using scanning electrochemical cell microscopy (SECCM), which allows electrochemical currents to be mapped at high spatial resolution across a surface for correlation with the corresponding structure and properties of the graphene surface. We establish that the rate of heterogeneous ET at graphene increases systematically with the number of graphene layers, and show that the stacking in multilayers also has a subtle influence on ET kinetics.

Graphene-based materials are having a huge impact in electrochemistry and electrochemical technologies, with promising applications in areas such as supercapacitors,[1] batteries,[2] electrocatalytic supports,[3] sensors for electroanalysis,[4] and transparent electrodes.[5] These important technologies typically use graphene produced by chemical vapor deposition (CVD)[6] and other scalable methods, yet important fundamental questions concerning heterogeneous electron transfer (ET) at such materials, intrinsic to many of these applications, remain to be addressed. Electrical measurements have revealed that the electron mobility[7] and the electronic band structure[8] are sensitive to the number of graphene layers and their stacking order, with implications for electrochemistry. In this communication, we thus seek to elucidate how both the number of graphene layers and arrangement of the layers influence heterogeneous ET kinetics.

Graphene grown by CVD on nickel substrates[9] (see Supporting Information (SI) section 1) was optimal for the present study because it presents a heterogeneous continuous layer of microsized multilayered flakes, which can be addressed with high resolution scanning electrochemical cell microscopy (SECCM).[10−13] Thus, on one sample it is possible to make thousands of individual electrochemical (EC) measurements at different locations and relate these to the corresponding graphene structure. This provides data sets on a scale that would be unfeasible with conventional photolithographic techniques of the type employed in recent EC studies of exfoliated graphene.[14−16] In order to study the unambiguous electrochemical response of graphene without any interference from a conductive substrate, CVD graphene layers were transferred to a silicon substrate with a 300 nm thermal grown oxide layer. This substrate allowed optical visualization and identification of the morphological film features characteristic of graphene,[17,18] for direct correlation with the local electrochemistry. Importantly, the approach described herein makes possible the study of graphene surfaces with minimal intrusion and avoids the need for any postprocessing lithographic step, which may result in unavoidable damage and possible interference of residues.[19]

Ferrocene derivatives have proven particularly suitable for the study of the ET activity of sp^2 carbon allotropes, such as carbon nanotubes,[15,19,20] and so we consider the one-electron oxidation of (ferrocenylmethyl) trimethylammonium ($FcTMA^{+/2+}$) as an exemplar outer-sphere redox couple. The dual channel theta pipet[21] (1.1 μm diameter) of the SECCM instrument was filled with an aqueous electrolyte solution containing 2 mM $FcTMA^+$ (as the hexafluorophosphate salt) and 30 mM KCl supporting electrolyte together with silver−silver chloride quasi counter reference electrodes (QCREs) to serve as both a conductance cell and voltammetric cell, with the graphene as the working electrode (WE) (Figure 1a). A linear sweep voltammogram (LSV) obtained with the SECCM setup (Figure 1b) demonstrates the electrochemical activity of graphene, with a sigmoidal wave for the oxidation of $FcTMA^+$ which rises with increasing potential to a clear transported-limited current ca. 68 pA. The waveshape is indicative of essentially reversible electron transfer (difference in the potentials at 3/4 and 1/4 of the limiting current, $E_{3/4} - E_{1/4} = 57$ mV). The wave highlights five different potentials at which the local electrochemical activity of CVD graphene was mapped by SECCM within the same area, yielding EC current maps (three of which are presented in Figure 1d and the others in SI section 2). These data show clearly that, at all potentials, the redox reaction occurs across the entire surface, but with significant heterogeneity in the current values. Simultaneously with the surface EC current, SECCM also acquires three complementary maps: z piezo displacement (related to the substrate topography), the ion conductance current between the QCREs in the barrels, and the AC component of the migration current (used as the set-point to control tip-to-sample separation).[10−13] Those maps (provided in SI section 2) confirm the stability of the electrolyte drop size (electrolyte contact area of the order of the pipet size,[12,21] here a 550 nm radius) and tip-to-sample separation (180 nm; see SI section 3, and ref 12). Thus, the changes in surface EC current can be assigned unequivocally to differences in EC activity of the material and not to any changes in wettability. This is further

Received: February 14, 2012
Published: April 9, 2012

   dx.doi.org/10.1021/ja3014902 | J. Am. Chem. Soc. 2012, 134, 7258−7261

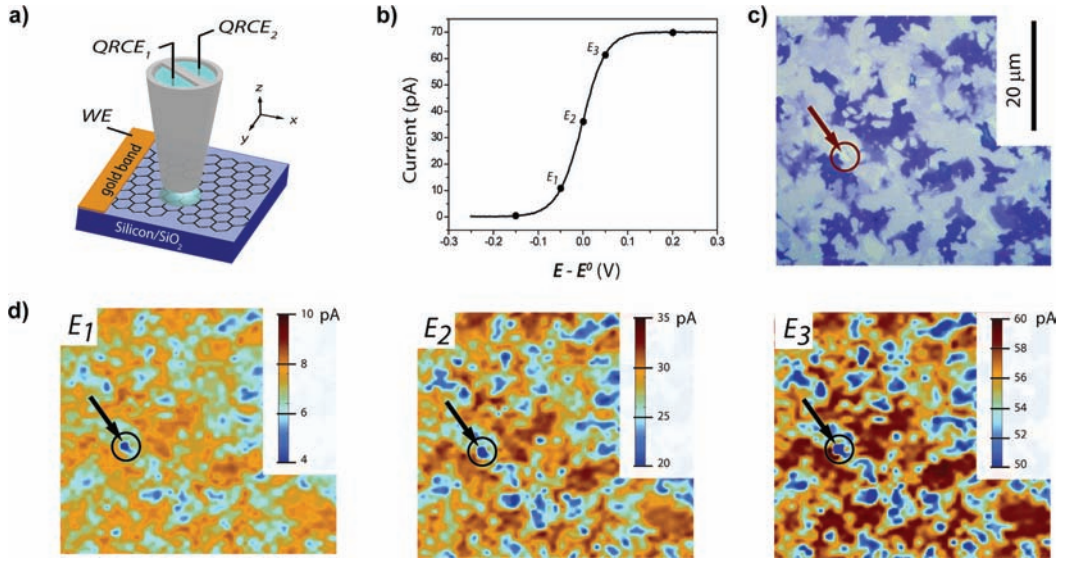

Figure 1. SECCM. (a) Schematic representation of the EC imaging setup. The graphene lies on a Si/SiO_2 substrate and is connected as the working electrode via an evaporated Cr/Au band. An SECCM probe is employed as a local and mobile EC cell for electrochemical imaging. (b) LSV for the oxidation of 2 mM $FcTMA^+$ (30 mM KCl) acquired with an SECCM setup on a graphene surface, at 100 mV s^{-1}, with a 1.1 μm diameter pipet. (c) Optical microscope image of the CVD graphene area mapped by SECCM, showing the heterogeneity of the surface and the presence of multiple-layer graphene flakes. (d) Set of three EC maps of the area shown in (c) acquired by SECCM at three different substrate electrode potentials ($E - E^\circ$) indicated in the LSV in (b) with labels E_1, E_2, and E_3. All images are at the same scale as (c). The arrow–circle in part (c) and (d) indicates a small area where the SiO_2 was exposed and measured currents in this area are below the lower limit on the scale bar. This area was used to calibrate the number of graphene layers (SI section 5).

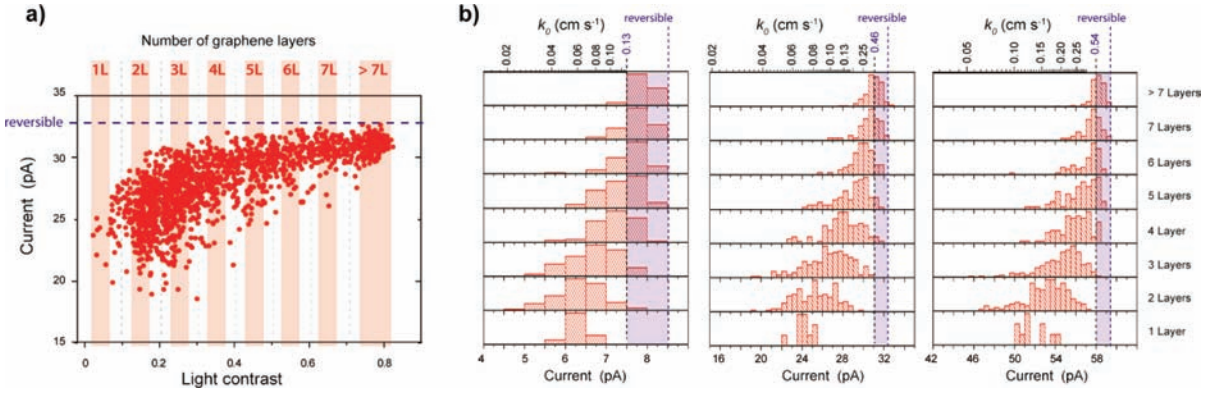

Figure 2. (a) Pixel-by-pixel correlation between the EC current map at potential E_2 and the number of graphene layers. (b) Histograms of the EC current and standard rate constant, k_0, for each defined number of CVD graphene layers, for potentials E_1, E_2, and E_3 (from left to right). The dashed line in (a) and the blue area in (b) denote the conditions where the ET process becomes entirely reversible.

evident by comparing the five EC maps (in Figure 1 and SI section 2) which show that the most active and inactive areas are in the same location in each map.

A finite element model[12] was developed to analyze the EC maps (SI section 3) and extract and assign standard heterogeneous ET rate constants at each micrometer-scale pixel of the images. For each pixel, we assumed reasonably the Butler–Volmer model for ET[22] and a uniformly active surface given the tiny area investigated. Electrochemical kinetic analyses are relatively insensitive to the value of the transfer coefficient for $\alpha = 0.5 \pm 0.2$ (ref 23), and so we chose $\alpha = 0.5$, given the large self-exchange ET rate constant for ferrocene and its derivatives.[24]

Comparison between the observed heterogeneity in EC activity of CVD graphene and the corresponding topography, revealed by optical microscopy or atomic force microscopy (AFM) (SI section 4), shows a clear correlation between electrochemical activity and the number of graphene layers. Qualitatively, there is close correspondence between dark regions (multilayers) in Figure 1c and high EC currents (Figure 1d and SI section 2).

In order to examine this relationship in more detail, EC current maps and the optical image were correlated quantitatively. Given the linear increase of green component contrast with the number of graphene layers,[9,17,18] and with further confirmation from micro-Raman spectroscopy (*vide infra*), the full range of light contrast was segmented into eight different bins assigned to a defined number of graphene layers (see SI section 5).

Figure 2a shows the local EC current at potential E_2 versus the number of graphene layers. Similar correlations at potentials E_1 and E_3 are provided in SI section 2. From this plot, it is clear that single layer graphene exhibits the lowest EC activity and that the activity increases systematically with the number of

dx.doi.org/10.1021/ja3014902 | J. Am. Chem. Soc. 2012, 134, 7258–7261

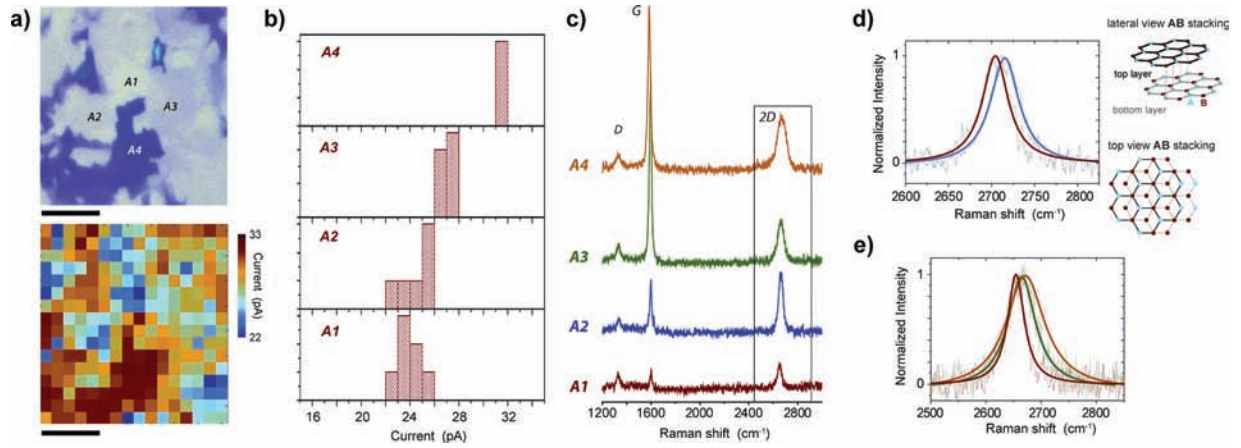

Figure 3. (a) Optical image of CVD graphene with four different flakes labeled A1, A2, A3, and A4, and corresponding SECCM data. Scale bar is 5 μm. (b) Histograms of the EC current in each designated flake at potential E_2. (c) Raman spectra acquired with an excitation wavelength of 633 nm and spot size of 500 nm at each graphene flake. The three characteristic Raman peaks for graphene are labeled as D, G, and 2D. (d) Raman 2D peak for regions A1 (red line) and A2 (blue line) plotted together highlighting the ~10 cm^{-1} Raman upshift characteristic for a non-AB stacking bilayer (blue line). Schematic of Bernal (AB-stacking) for a bilayer of graphene. The basic structure of graphene is defined with two atoms in the unit cell, denoted A (red dot) and B (blue dot). For an AB stacking bilayer, the A atom of the top layer lies directly over the B atom of the bottom layer. (e) The Raman 2D peak for areas A1 (red line), A3 (green line), and A4 (orange line).

layers, to a situation where the flakes are so active that the ET process becomes essentially reversible[13] within experimental error (see SI, Figure S9).

EC current distributions were analyzed to obtain the corresponding ET standard rate constants (k_0) for potentials E_1, E_2, and E_3 (full details in ref 12 and SI section 3). Figure 2b reveals that the ET kinetics evolves with the number of layers toward faster ET and a broader range of k_0 (and current magnitudes) from monolayer to multilayer graphene. This is found consistently at all three potentials. Although there will be some cross contribution of different flakes at some single point measurements (where the tip is at the boundary between flakes), the different stacking order within the graphene multilayers could also play a role in the broadness of ET kinetics, seen for bilayer, trilayer, and thicker flakes, especially for epitaxy of CVD multilayer graphene, where non-Bernal or AB stacking order is very common.[25]

Raman spectroscopy was employed to determine both the stacking order and the corresponding number of layers on different graphene flakes for correlation with EC (Figure 3). Figure 3a shows a zoom of the optical image and the associated SECCM map. We differentiate four different graphene flakes labeled A1, A2, A3, and A4, categorized as monolayer, bilayer, trilayer, and multilayer graphene, respectively (*vide infra*). The Raman spectra of those areas (Figure 3c) present the three characteristic graphene D, G, and 2D peaks.[26] For the A1 and A2 areas, the 2D bands are slightly more intense than the G peak, and the FWHM values of the 2D peaks are around 35−40 cm^{-1}, hallmarks of single layer CVD graphene.[9,27] However, the upshift of about 10 cm^{-1} (refs 28, 29) for the 2D peak (Figure 3d), in addition to light contrast values of 0.15 (SI section 5), indicate that the A2 region actually corresponds to a non-AB stacking bilayer. The lack of AB stacking (Figure 3d) reduces electronic coupling between the graphene layers, so that bilayer graphene in this configuration has electronic properties similar to those of monolayer graphene.[30−32] This evidently directly impacts the EC activity: current values for the A2 spot are very similar to those of the A1 region (Figure 3b and SI section 6), which corresponds to a single layer. It is accepted that the electronic structure and density of states play a key role in heterogeneous ET rates,[22,33] and these results show that different graphene layers (monolayer and bilayer), with closely similar band structures, behave analogously in terms of electrochemistry. This result also allows us to rule out a strong influence of charge carrier mobility to the EC activity measured. An increase of mobility is expected for a non-AB stacking bilayer, compared to monolayer graphene, since the substrate effect is, to some extent, screened by the additional graphene layer beneath the top layer in the case of bilayer graphene,[34] but this does not enhance ET kinetics compared to the intrinsic activity of monolayer graphene.

The areas A3 and A4 are assigned to trilayer and multilayer (>trilayer), respectively, based on the much broader 2D peak (Figure 3e) and the intensity and peak position of the G peak (Figure 3c). For these domains, an increase of EC activity is observed with the number of layers (Figure 3b), consistent with the evolution of the density of electronic states through single layer, AB-bilayer, and trilayer graphene.[7] These more detailed analyses (Figure 3b and SI section 6) confirm the trend (*vide supra*) between EC current and light contrast in the optical image (interpreted as the number of graphene layers).

Complementary experiments were carried out to eliminate other possible causes for the observed changes in EC activity with the number of graphene layers. An exhaustive analysis of surface roughness was performed over the sample with AFM (SI section 4) to discard the possibility that the observed increase of EC activity was due to a change in the roughness of the surface with the number of layers. The presence of wrinkles is unavoidable for synthetic graphene, which are responsible for local changes in the electronic structure,[35] but they were essentially uniform (as evidenced by AFM in SI) over the entire surface area and independent of the number of layers and flakes. The Raman D peak at 1350 cm^{-1} is usually used to determine the density of defects on graphene,[26,27] either as the peak intensity itself or with the ratio of D and G peaks (I_D/I_G). In all spectra obtained, the D peak intensity was essentially constant for all flakes studied and independent of the number of layers. Indeed, if the I_D/I_G ratios are compared, the multilayered flakes have the lowest density of defects, yet have higher activity. It is further well-known[36,37] that edges

dx.doi.org/10.1021/ja3014902 | J. Am. Chem. Soc. 2012, 134, 7258−7261

accumulate a higher density of defects, but it is clear that we see no increase of EC activity either along the edges of the flakes or at the (step-edge) boundary between flakes, at the spatial resolution of the investigation.

In conclusion, we have demonstrated how the ET activity of a complex graphene material can be elucidated, analyzed, and correlated with intrinsic structural properties using high resolution SECCM in tandem with Raman microscopy, optical microscopy, and AFM. The unprecedented insights on the structural controls of ET are of fundamental value and provide a rational basis for the design and use of graphene in electrochemical technologies. The SECCM methodology described is general, and we expect it will find increasing use for structure−function imaging of surface and interfacial processes.

■ ASSOCIATED CONTENT

Supporting Information

Full experimental details of graphene synthesis, SECCM operation and complementary maps, AFM images, light contrast calibration, and FEM simulations. This material is available free of charge via the Internet at http://pubs.acs.org.

■ AUTHOR INFORMATION

Corresponding Author

p.r.unwin@warwick.ac.uk

Notes

The authors declare no competing financial interest.

■ ACKNOWLEDGMENTS

This project was supported by the European Research Council through Project ERC-2009-AdG 247143-QUANTIF and a Marie Curie IntraEuropean Fellowship (236885) (A.G.G.). Funding from the EPSRC (EP/H023909/1) and UK National Physical Laboratory is also acknowledged. Equipment used in this research was obtained through Science City (AM2), with support from Advantage West Midlands and partial funding by the European regional Development Fund. The authors thank Mr. Kim McKelvey for assistance in data analysis and Mr. Tom Miller and Mr. Anatolii Kuharuk for contributions to CVD graphene synthesis.

■ REFERENCES

(1) Zhu, Y.; Murali, S.; Stoller, M. D.; Ganesh, K. J.; Cai, W.; Ferreira, P. J.; Pirkle, A.; Wallace, R. M.; Cychosz, K. A.; Thommes, M.; Su, D.; Stach, E. A.; Ruoff, R. S. *Science* **2011**, *332*, 1537.

(2) Xiao, J.; Mei, D.; Li, X.; Xu, W.; Wang, D.; Graff, G. L.; Bennett, W. D.; Nie, Z.; Saraf, L. V.; Aksay, I. A.; Liu, J.; Zhang, J.-G. *Nano Lett.* **2011**, *11*, 5071.

(3) Liang, Y.; Li, Y.; Wang, H.; Zhou, J.; Wang, J.; Regier, T.; Dai, H. *Nat. Mater.* **2011**, *10*, 780.

(4) Schedin, F.; Geim, A. K.; Morozov, S. V.; Hill, E. W.; Blake, P.; Katsnelson, M. I.; Novoselov, K. S. *Nat. Mater.* **2007**, *6*, 652.

(5) Bonaccorso, F.; Sun, Z.; Hasan, T.; Ferrari, A. C. *Nat. Photonics* **2010**, *4*, 611.

(6) Bae, S.; Kim, H.; Lee, Y.; Xu, X.; Park, J.-S.; Zheng, Y.; Balakrishnan, J.; Lei, T.; Ri Kim, H.; Song, Y. I.; Kim, Y.-J.; Kim, K. S.; Ozyilmaz, B.; Ahn, J.-H.; Hong, B. H.; Iijima, S. *Nat. Nanotechnol.* **2010**, *5*, 574.

(7) Zhu, W.; Perebeinos, V.; Freitag, M.; Avouris, P. *Phys. Rev. B* **2009**, *80*, 235402.

(8) Bao, W.; Jing, L.; Velasco, J.; Lee, Y.; Liu, G.; Tran, D.; Standley, B.; Aykol, M.; Cronin, S. B.; Smirnov, D.; Koshino, M.; McCann, E.; Bockrath, M.; Lau, C. N. *Nat. Phys.* **2011**, *7*, 948.

(9) Reina, A.; Jia, X.; Ho, J.; Nezich, D.; Son, H.; Bulovic, V.; Dresselhaus, M. S.; Kong, J. *Nano Lett.* **2009**, *9*, 30.

(10) Ebejer, N.; Schnippering, M.; Colburn, A. W.; Edwards, M. A.; Unwin, P. R. *Anal. Chem.* **2010**, *82*, 9141.

(11) Lai, S. C.; Dudin, P. V.; Macpherson, J. V.; Unwin, P. R. *J. Am. Chem. Soc.* **2011**, *133*, 10744.

(12) Snowden, M. E.; Güell, A. G.; Lai, S. C.; McKelvey, K.; Ebejer, N.; O'Connell, M. A.; Colburn, A. W.; Unwin, P. R. *Anal. Chem.* **2012**, *84*, 2483.

(13) Lai, S. C. S.; Patel, A. N.; McKelvey, K.; Unwin, P. R. *Angew. Chem., Int. Ed.* **2012**, DOI: 10.1002/201200564.

(14) Xia, J.; Chen, F.; Li, J.; Tao, N. *Nat. Nanotechnol.* **2009**, *4*, 505.

(15) Li, W.; Tan, C.; Lowe, M. A.; Abruña, H. c. D.; Ralph, D. C. *ACS Nano* **2011**, *5*, 2264.

(16) Valota, A. T.; Kinloch, I. A.; Novoselov, K. S.; Casiraghi, C.; Eckmann, A.; Hill, E. W.; Dryfe, R. A. W. *ACS Nano* **2011**, *5*, 8809.

(17) Blake, P.; Hill, E. W.; Neto, A. H. C.; Novoselov, K. S.; Jiang, D.; Yang, R.; Booth, T. J.; Geim, A. K. *Appl. Phys. Lett.* **2007**, *91*, 063124.

(18) Ni, Z. H.; Wang, H. M.; Kasim, J.; Fan, H. M.; Yu, T.; Wu, Y. H.; Feng, Y. P.; Shen, Z. X. *Nano Lett.* **2007**, *7*, 2758.

(19) Dudin, P. V.; Snowden, M. E.; Macpherson, J. V.; Unwin, P. R. *ACS Nano* **2011**, *5*, 10017.

(20) Heller, I.; Kong, J.; Heering, H. A.; Williams, K. A.; Lemay, S. G.; Dekker, C. *Nano Lett.* **2004**, *5*, 137.

(21) Rodolfa, K. T.; Bruckbauer, A.; Zhou, D.; Korchev, Y. E.; Klenerman, D. *Angew. Chem., Int. Ed.* **2005**, *44*, 6854.

(22) Bard, A. J.; Faulkner, L. *Electrochemical methods: fundamentals and applications*; Wiley: Weinheim, 2001.

(23) Mirkin, M. V.; Bard, A. J. *Anal. Chem.* **1992**, *64*, 2293.

(24) Nielson, R. M.; McManis, G. E.; Safford, L. K.; Weaver, M. J. *J. Phys. Chem.* **1989**, *93*, 2152.

(25) Pimenta, M. A.; Dresselhaus, G.; Dresselhaus, M. S.; Cancado, L. G.; Jorio, A.; Saito, R. *Phys. Chem. Chem. Phys.* **2007**, *9*, 1276.

(26) Ferrari, A. C.; Meyer, J. C.; Scardaci, V.; Casiraghi, C.; Lazzeri, M.; Mauri, F.; Piscanec, S.; Jiang, D.; Novoselov, K. S.; Roth, S.; Geim, A. K. *Phys. Rev. Lett.* **2006**, *97*, 187401.

(27) Malard, L. M.; Pimenta, M. A.; Dresselhaus, G.; Dresselhaus, M. S. *Phys. Rep.* **2009**, *473*, 51.

(28) Poncharal, P.; Ayari, A.; Michel, T.; Sauvajol, J. L. *Phys. Rev. B.* **2008**, *78*, 113407.

(29) Ni, Z.; Wang, Y.; Yu, T.; You, Y.; Shen, Z. *Phys. Rev. B.* **2008**, *77*, 235403.

(30) Lopes dos Santos, J. M. B.; Peres, N. M. R.; Castro Neto, A. H. *Phys. Rev. Lett.* **2007**, *99*, 256802.

(31) Latil, S.; Meunier, V.; Henrard, L. *Phys. Rev. B* **2007**, *76*, 201402.

(32) Hass, J.; Varchon, F.; Millán-Otoya, J. E.; Sprinkle, M.; Sharma, N.; de Heer, W. A.; Berger, C.; First, P. N.; Magaud, L.; Conrad, E. H. *Phys. Rev. Lett.* **2008**, *100*, 125504.

(33) Heller, I.; Kong, J.; Williams, K. A.; Dekker, C.; Lemay, S. G. *J. Am. Chem. Soc.* **2006**, *128*, 7353.

(34) Ohta, T.; Bostwick, A.; McChesney, J. L.; Seyller, T.; Horn, K.; Rotenberg, E. *Phys. Rev. Lett.* **2007**, *98*, 206802.

(35) Xu, K.; Cao, P.; Heath, J. R. *Nano Lett.* **2009**, *9*, 4446.

(36) Graf, D.; Molitor, F.; Ensslin, K.; Stampfer, C.; Jungen, A.; Hierold, C.; Wirtz, L. *Nano Lett.* **2007**, *7*, 238.

(37) Yu, Q.; Jauregui, L. A.; Wu, W.; Colby, R.; Tian, J.; Su, Z.; Cao, H.; Liu, Z.; Pandey, D.; Wei, D.; Chung, T. F.; Peng, P.; Guisinger, N. P.; Stach, E. A.; Bao, J.; Pei, S.-S.; Chen, Y. P. *Nat. Mater.* **2011**, *10*, 443.